Supporting Information

High-Performance Aramid Electrodes for High-Rate and Long Cycle-Life Organic Li-ion Battery

Febri Baskoro,[a] Hong-Jhen Lin,[a] Cha-Wen Chang,[b] Ching-Lan Wang,[a,c] Andre Lammiduk Lubis,[a] and Hung-Ju Yen,[a]*

[a] Institute of Chemistry, Academia Sinica, 128 Academia Road, Section 2, Nankang, Taipei 11529, Taiwan
[b] Department of Interface Chemistry, Division of Applied Chemistry, Material and Chemical Research Laboratories, Industrial Technology Research Institute, Hsinchu 30011, Taiwan.
[c] Department of Chemical Engineering, National Taiwan University of Science and Technology, Taipei 106, Taiwan.

E-mail: hjyen@gate.sinica.edu.tw

Supplementary Notes:

Supplementary Note 1 - Diffusion coefficient calculation based on EIS spectra

EIS is a powerful tool to investigate electrical properties of materials surface in association with physicochemical processes such as charge transfer of electronic and ionic charge carriers, mass transport through diffusion and convection.[1] The Nyquist plots typically can be divided into three sections, namely high, mid and low frequency regions. The high frequency region reflected the conduction through electrolyte, separator and wires.[2] The mid frequency region is related to the charge transfer and the kinetic reactions.[3, 4] The low frequency region in which usually featured by 45° slope, represents the diffusion limited region in the solid phase and is typically characterized by the Warburg impedance.[5, 6] Basically, there are two equations that define Warburg impedance[7]:

$$Z' = \sigma/\omega^{\frac{1}{2}} - j\,\sigma/\omega^{\frac{1}{2}}$$

$$\left| -Z'' \right| = \sqrt{2}\,\sigma/\omega^{\frac{1}{2}}$$

where Z′ and Z′′are real and imaginary impedance, respectively. ω is the angular frequency and σ is the Warburg coefficient. Therefore, The Warburg coefficient (σ) can be determine by the slope of Warburg plot (Z′ vs $1/\omega^{\frac{1}{2}}$). Meanwhile, the relationship of Warburg coefficient (σ) and the diffusion coefficient is given by[7]:

$$\sigma = \frac{RT}{n^2F^2A\sqrt{2}}\left(\frac{1}{D_O^{\frac{1}{2}}C_O^b} + \frac{1}{D_R^{\frac{1}{2}}C_R^b}\right)$$

where R is ideal gas constant, T is absolute temperature, n is the number of electron transferred, F is Faraday's constant, A is the area of the electrode, D_O and D_R are the

diffusivity of oxidation and reduction species, respectively. Then C_O and C_R are the concentration of oxidation and reduction species, respectively. In addition, because of the fact that only Li^+ which moving inside of graphite electrode, the Warburg coefficient (σ) can be simplified by :

$$\sigma = \frac{RT}{n^2F^2A\sqrt{2}}\left(\frac{1}{D_{Li}^{1/2}C_{Li}}\right)$$

where D_{Li} and C_{Li} are the diffusion coefficient and concentration of Li^+.

Supplementary Note 2 - Sweep rate voltammetry for charge-stored characteristic

In the battery system, there are consecutive electrochemical reactions occurs in the electrodes. The sweep rate voltammetry is one of powerful technique to probe those reactions. The total stored charge in a CV curve generally can be separate into three components: (a) the faradaic contribution from the Li^+ ion insertion process; (b) the faradaic contribution from the charge-transfer process with surface atoms, referred to as pseudocapacitance; (c) the non-faradaic contribution from the double layer effect.[8, 9]

In addition, the contribution of both types capacitive effects, pseudocapacitance and double layer effect, can be substantial due to the increasing surface area of the electrode.[8] These faradaic contribution from insertion process (diffusion control) and capacitive effects can be characterized using CV data at various scan rates (see Fig. 3) and expressed by following formula:

$$i = av^b$$

where *i* is current response to the scan rate *v*, while *a* and *b* are constants. The *b* value can be obtained from the slope of *log i* vs *log v*, see Fig. S16a. In addition, if the *b* value close to 0.5 would indicate half-infinite linear diffusion controlled process, meanwhile *b* value close to 1 indicates the current is surface controlled.[8, 10-12] Since the *b* value is the sum of faradaic response of diffusion controlled and capacitive effects, a closer examination from sweep rate voltammetry can be applied to quantify the capacitive effects (k_1v) and diffusion controlled behavior ($k_2v^{1/2}$) by following formula[8, 9, 11, 13]:

$$i = k_1v + k_2v^{1/2}$$

The k_1 and k_2 values can be determined by plotting $i/v^{1/2}$ vs $v^{1/2}$ (see Fig. S16b).

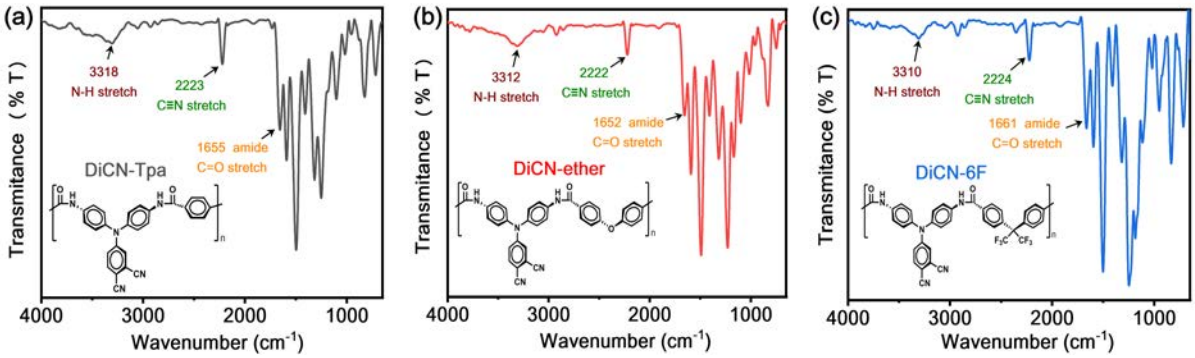

Fig. S1. The FTIR spectra of DiCN-aramids. (a) **DiCN-Tpa**. (b) **DiCN-Ether**. (c) **DiCN-6F**.

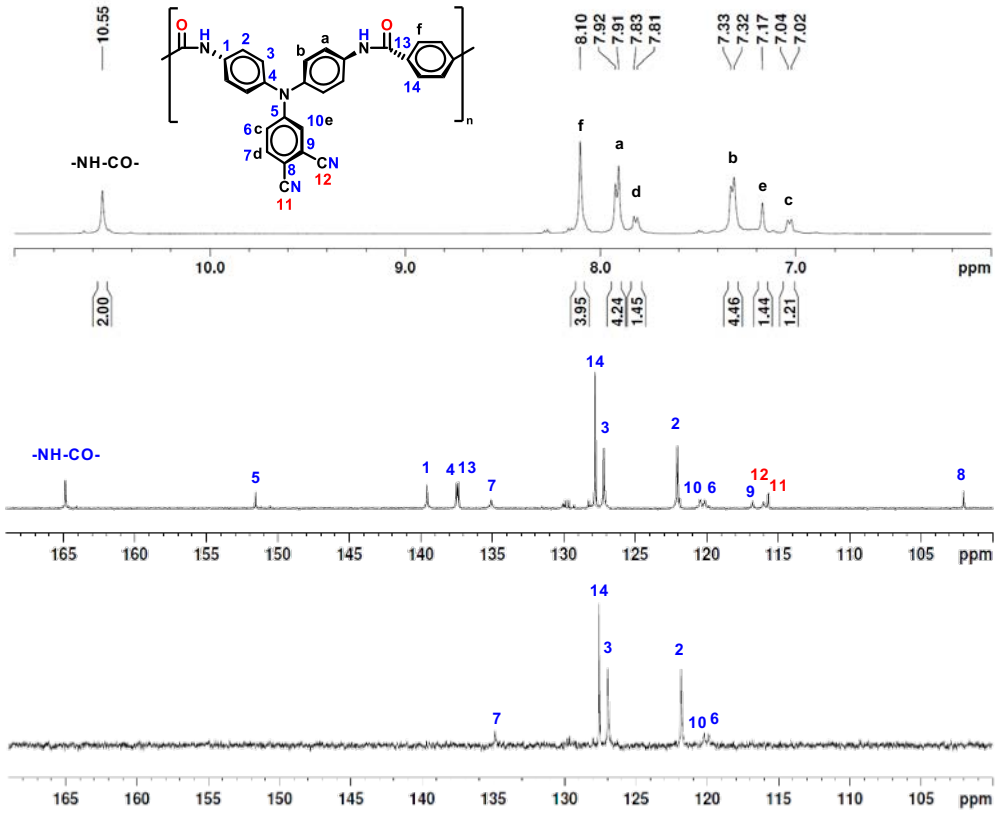

Fig. S2. ^{1}H and ^{13}C NMR spectra of aramid **DiCN-Tpa** in DMSO-d_6.

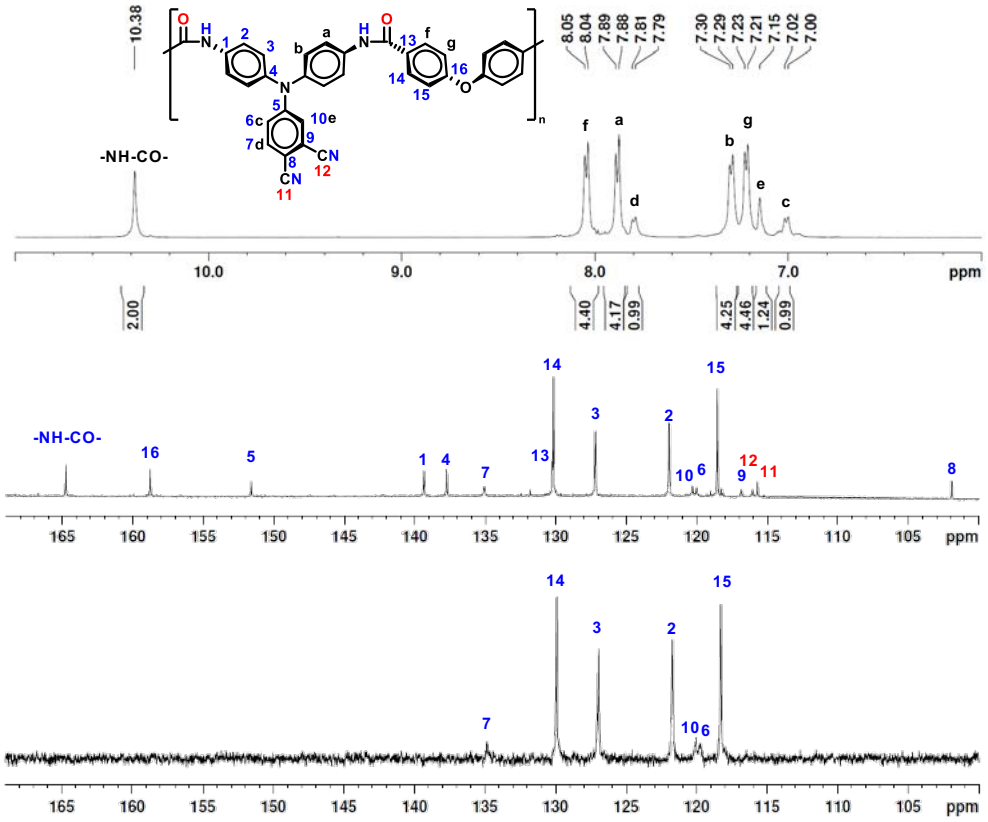

Fig. S3. ^{1}H and ^{13}C NMR spectra of aramid **DiCN-Ether** in DMSO-d_6.

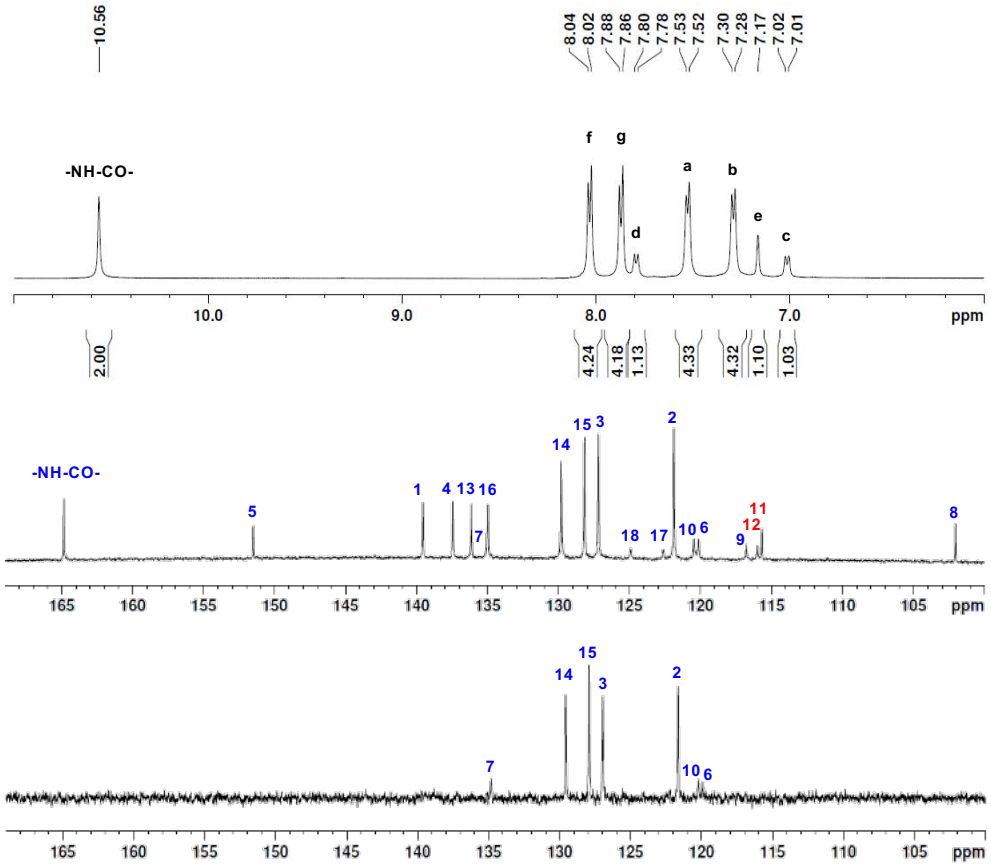

Fig. S4. ^{1}H and ^{13}C NMR spectra of aramid **DiCN-6F** in DMSO-d_6.

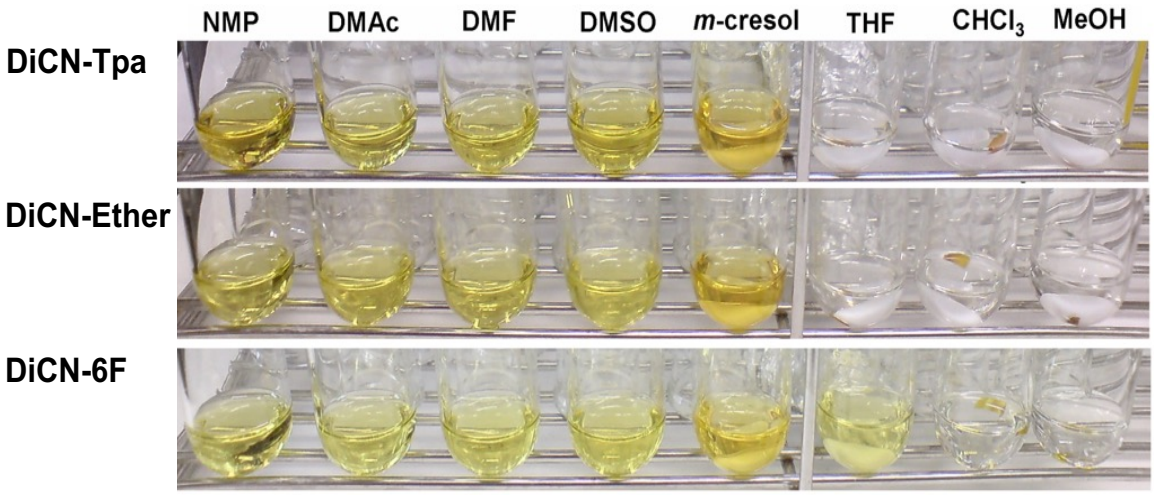

Fig. S5. Solubility test of DiCN-aramids in various solvents.

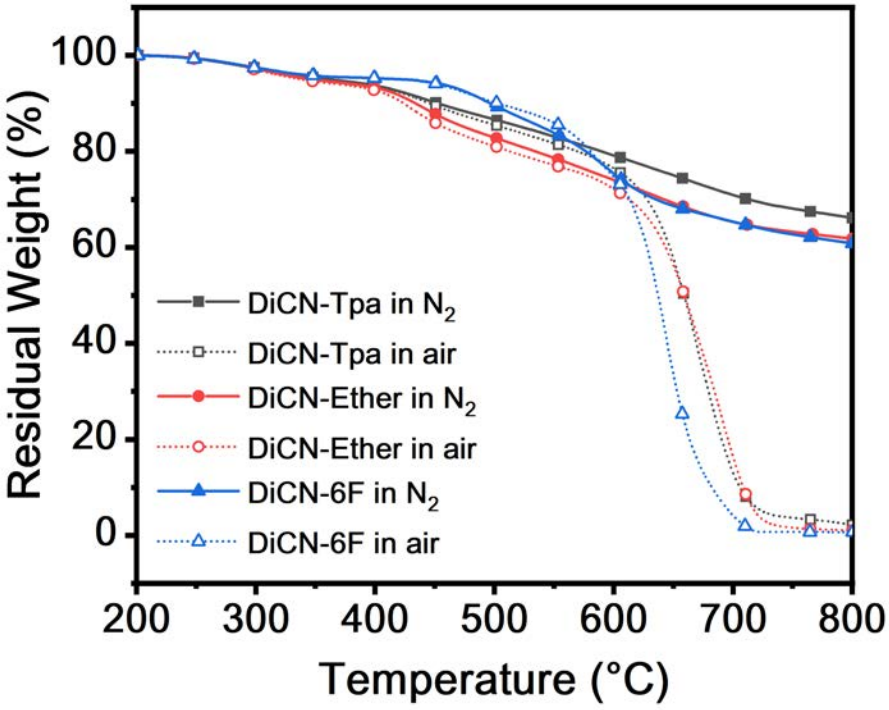

Fig. S6. TGA thermograms of aramids in both air and nitrogen at a scan rate of 20 °C/min.

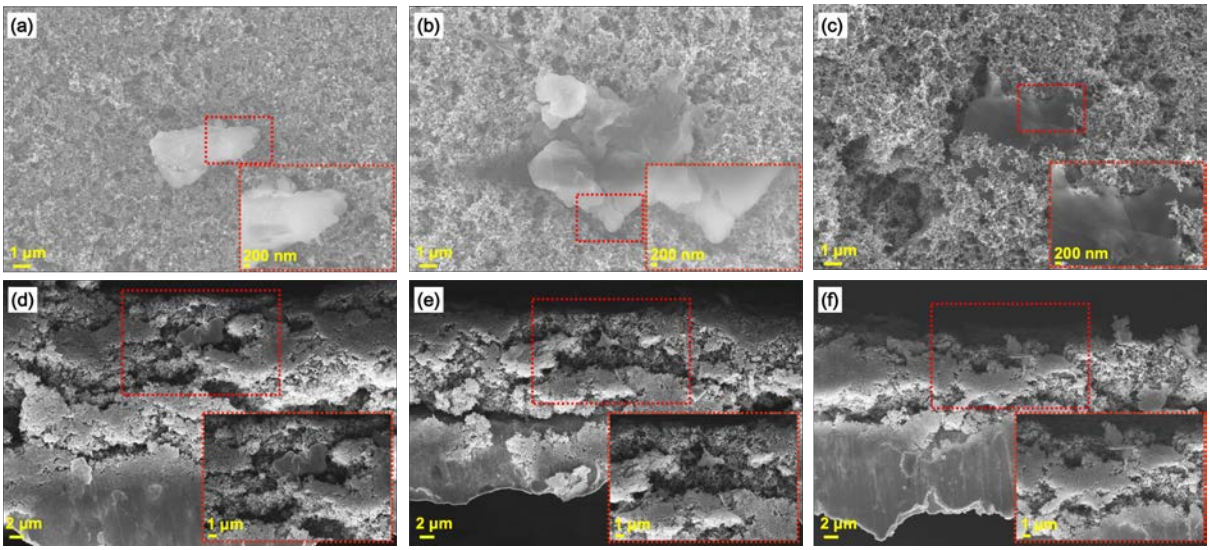

Fig. S7. The surface and cross-sectional FESEM images of DiCN-aramids before cycling. (a and d) **DiCN-Tpa**. (b and e) **DiCN-Ether**. (c and f) **DiCN-6F**. The inset figures are the zoom in images from red-dashed square area.

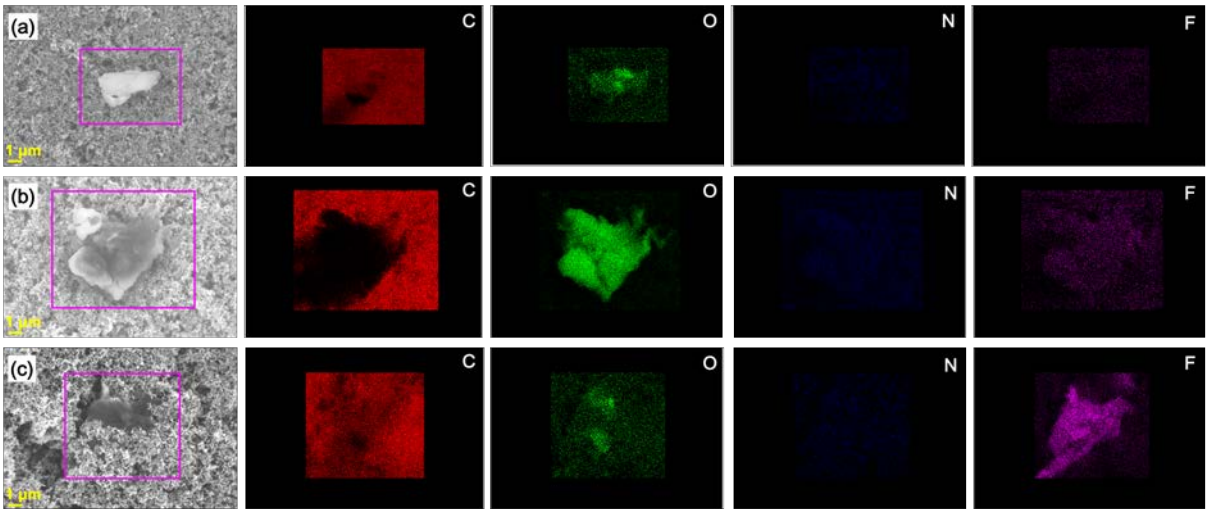

Fig. S8. The FESEM-EDS mapping of DiCN-aramids before cycling. (a) **DiCN-Tpa**. (b) **DiCN-Ether**. (c) **DiCN-6F**. The different color represent different element in the images: Red (Carbon); Green (Oxygen); Blue (Nitrogen); and Magenta (Fluorine).

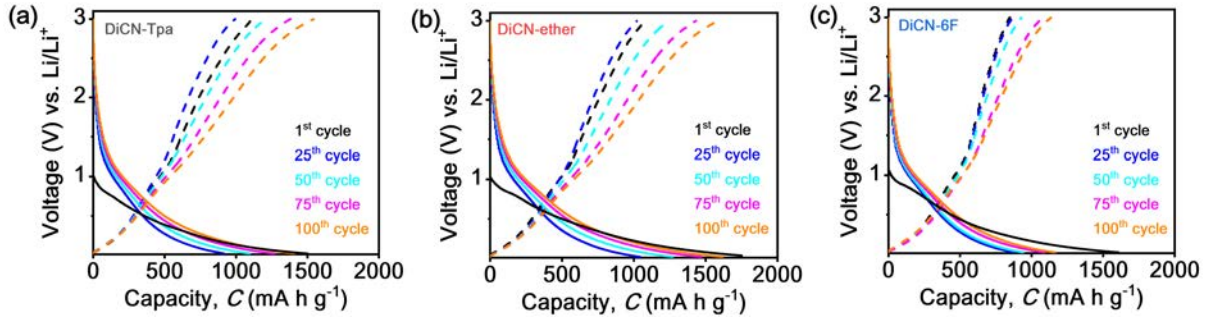

Fig. S9. The galvanostatic profile of DiCN-aramids at 0.1 A g^{-1} current density. (a) **DiCN-Tpa**. (b) **DiCN-Ether**. (c) **DiCN-6F**.

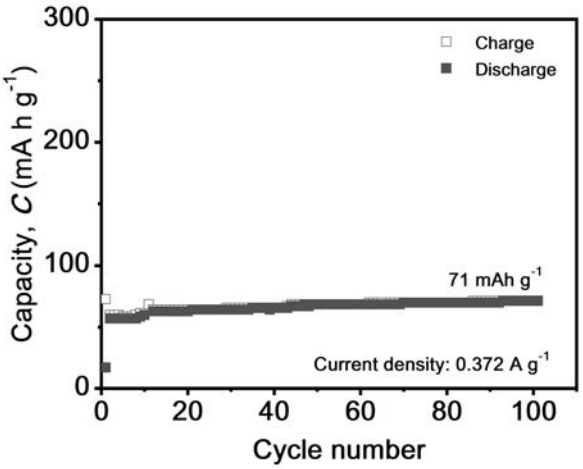

Fig. S10. The cycling performance of Super-P anode at 0.372 A g^{-1}.

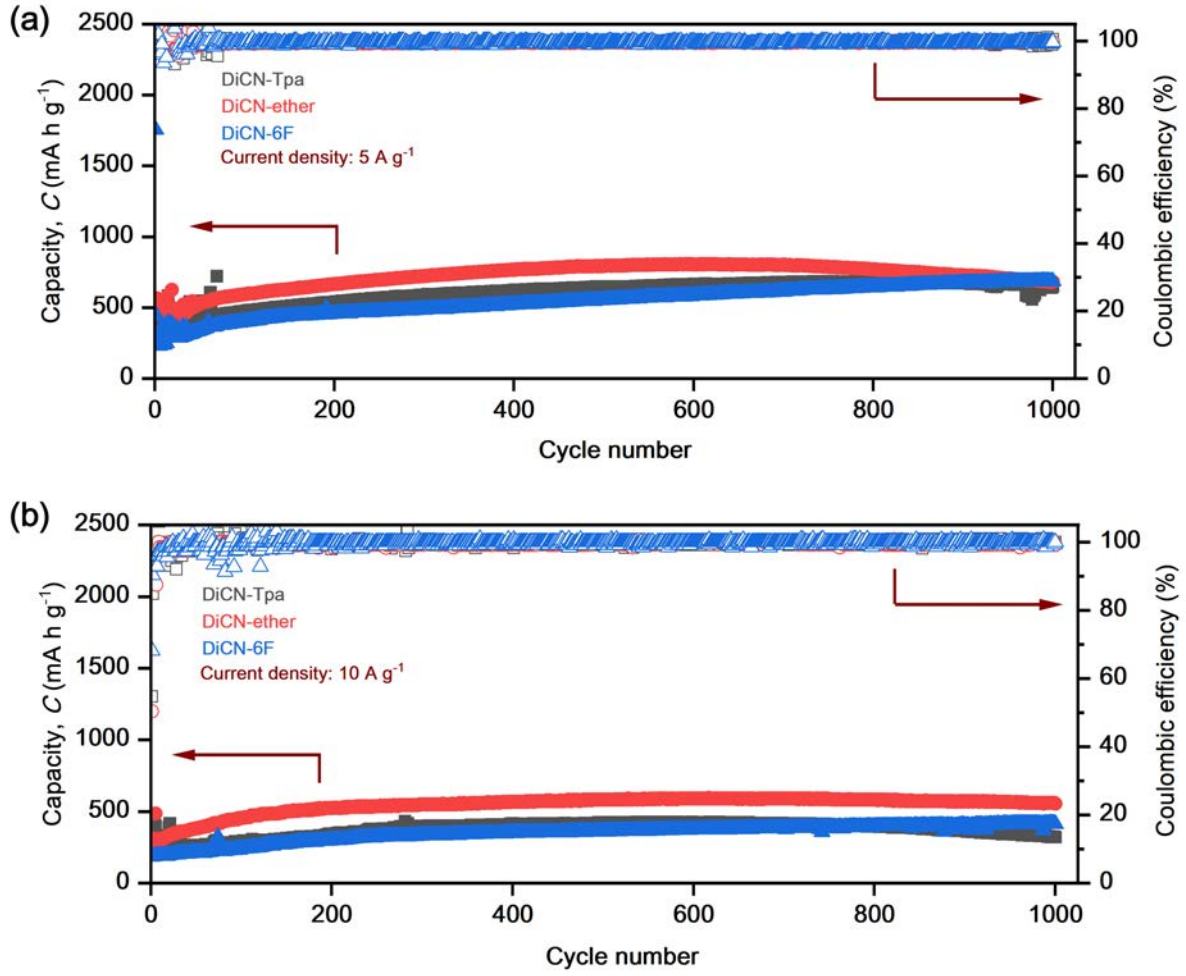

Fig. S11. The long cycling performance of DiCN-aramids at (a) 5 and (b) 10 A g^{-1}, respectively.

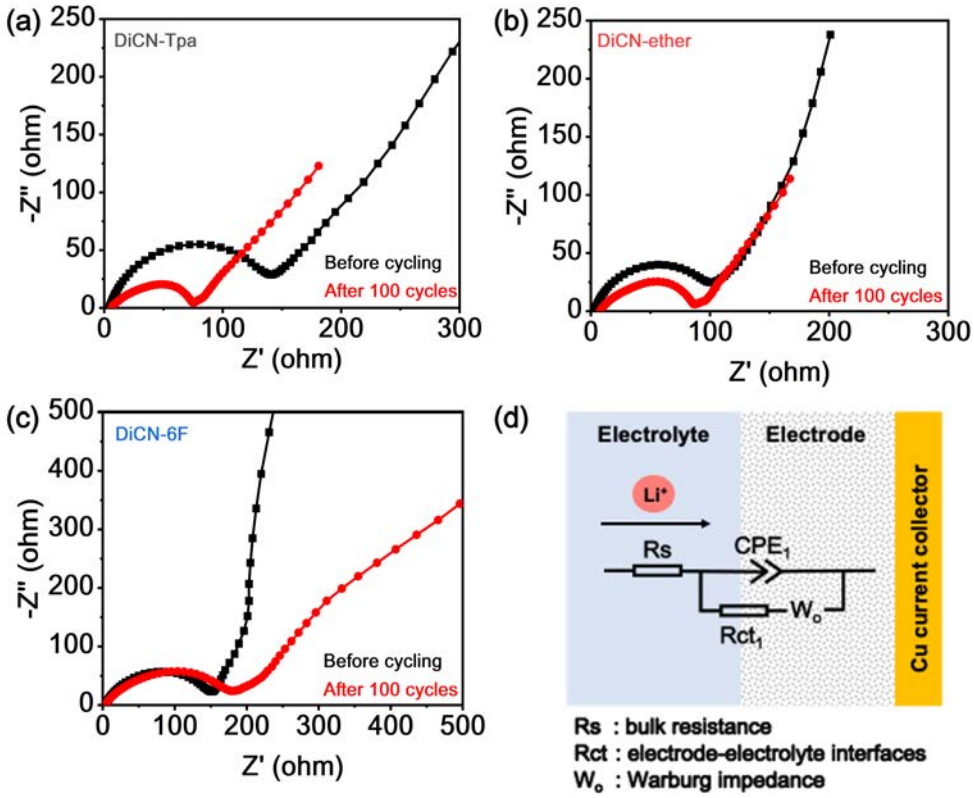

Fig. S12. Nyquist plots of the DiCN-aramid electrodes before and after 100 cycles: (a) **DiCN-Tpa**; (b) **DiCN-Ether**; (c) **DiCN-6F**, respectively. (d) Electrical circuit used to fit the EIS data.

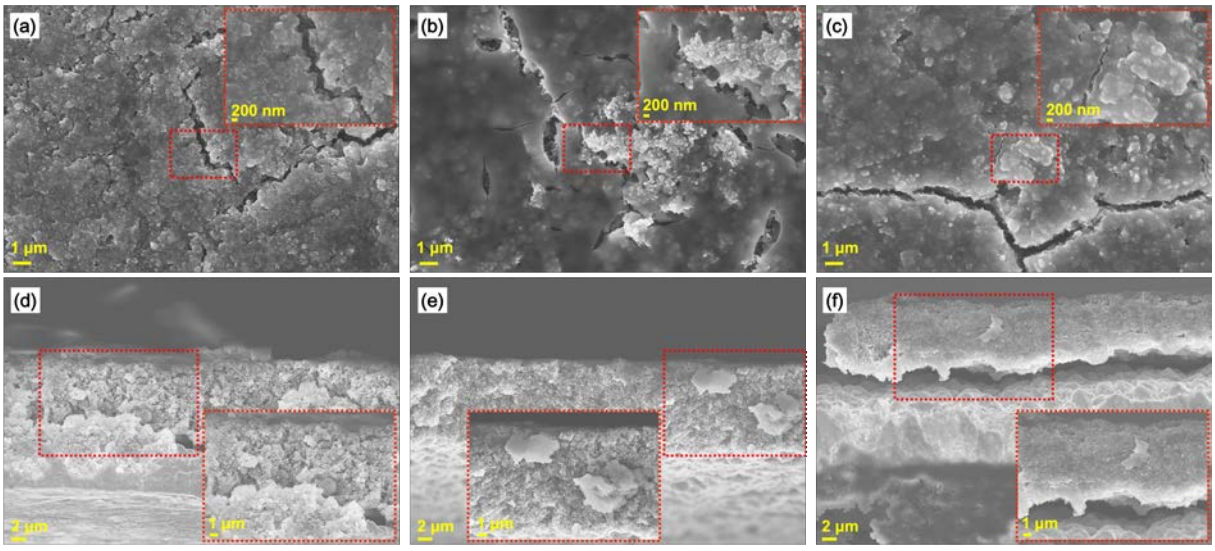

Fig. S13. The surface and cross-sectional FESEM images of DiCN-aramids after 100 cycles. (a and d) **DiCN-Tpa**. (b and e) **DiCN-Ether**. (c and f) **DiCN-6F**. The inset figures are the zoom in images from red-dashed square area.

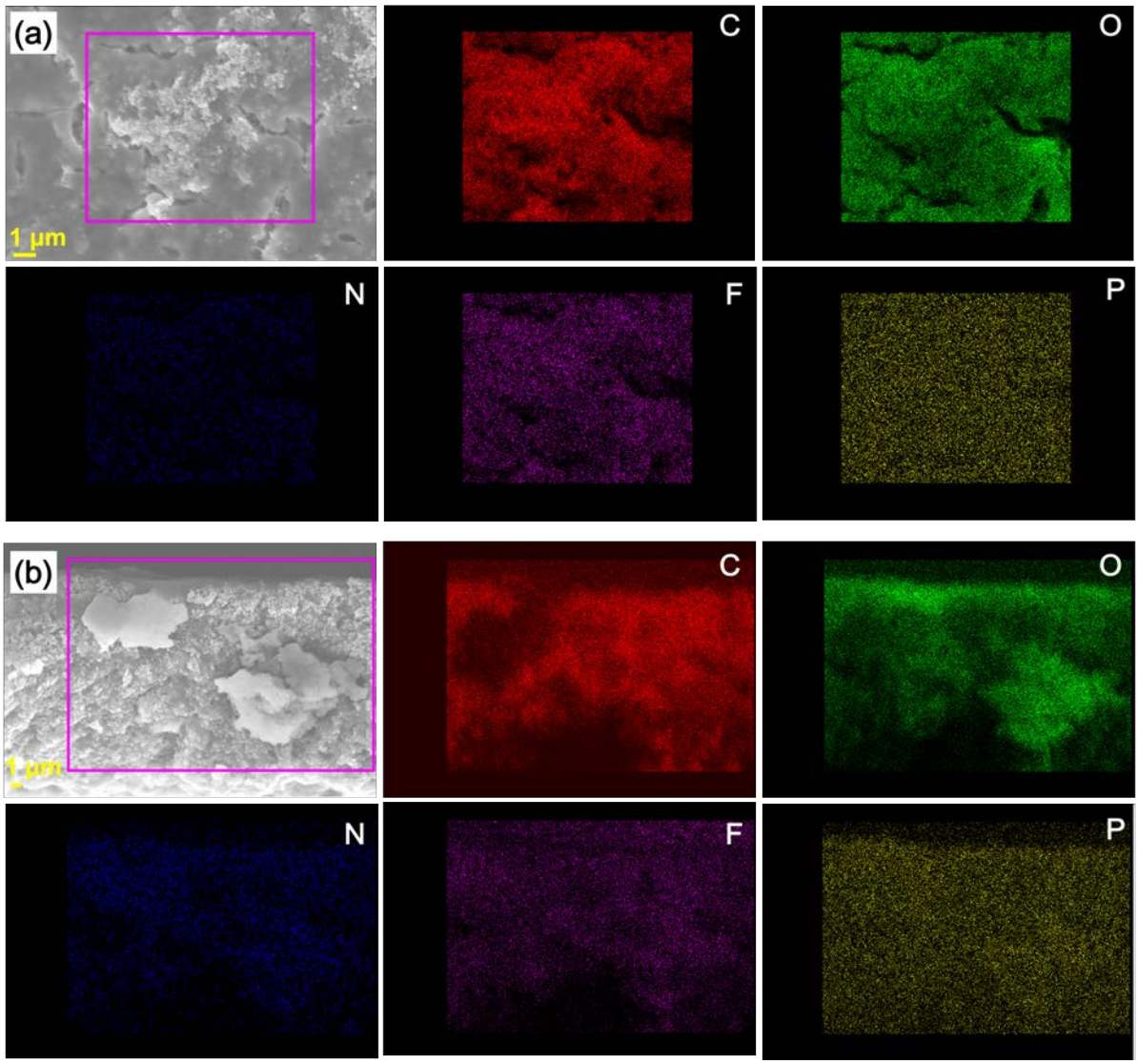

Fig. S14. The FESEM-EDS mapping of **DiCN-Ether** after 100 cycles. (a) Surface. (b) Cross-section. The different color represent different element in the images: Red (Carbon); Green (Oxygen); Blue (Nitrogen); Magenta (Fluorine); and Yellow (Phosphor).

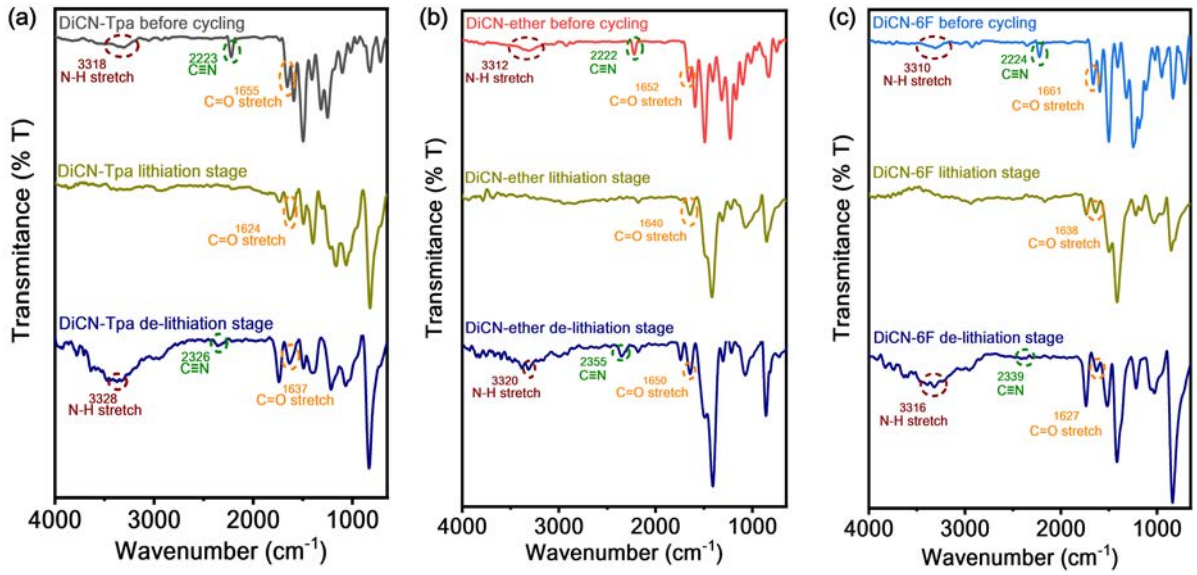

Fig. S15. The ex-situ FTIR spectra of DiCN-aramids at various stages during electrochemical process. (a) **DiCN-Tpa**. (b) **DiCN-Ether**. (c) **DiCN-6F**.

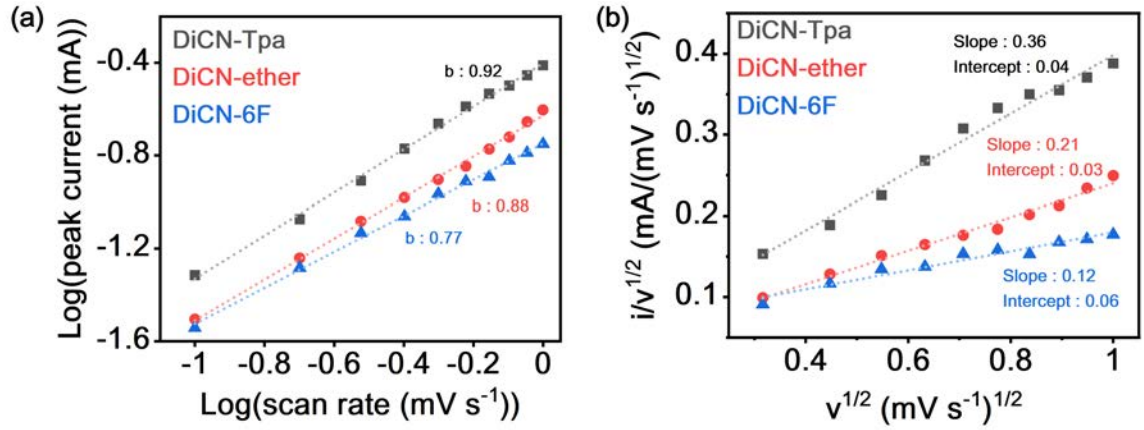

Fig. S16. (a) The *b* value as slope function of Log scan rate (*v*) vs Log peak current (*i*) for DiCN-aramids. (b) The $k_1$value as slope function of $v^{1/2}$ vs $i/v^{1/2}$ for DiCN-aramids.

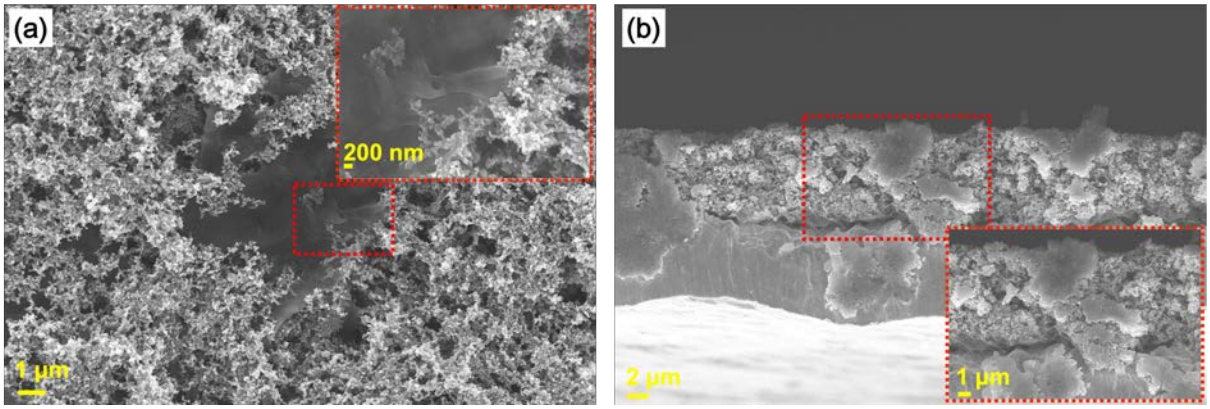

Fig. S17. The FESEM images of binder-free **DiCN-Ether** before cycling. (a) Surface. (b) Cross-section. The inset figures are the zoom in images from red-dashed square area.

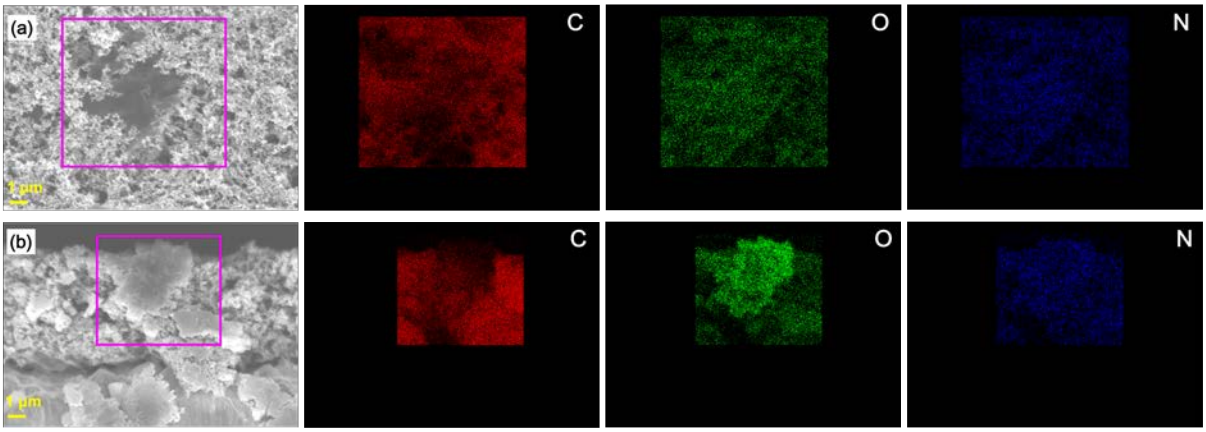

Fig. S18. The FESEM-EDS mapping of binder-free **DiCN-Ether** before cycling. (a) Surface. (b) Cross-section. The different color represent different element in the images: Red (Carbon); Green (Oxygen); and Blue (Nitrogen).

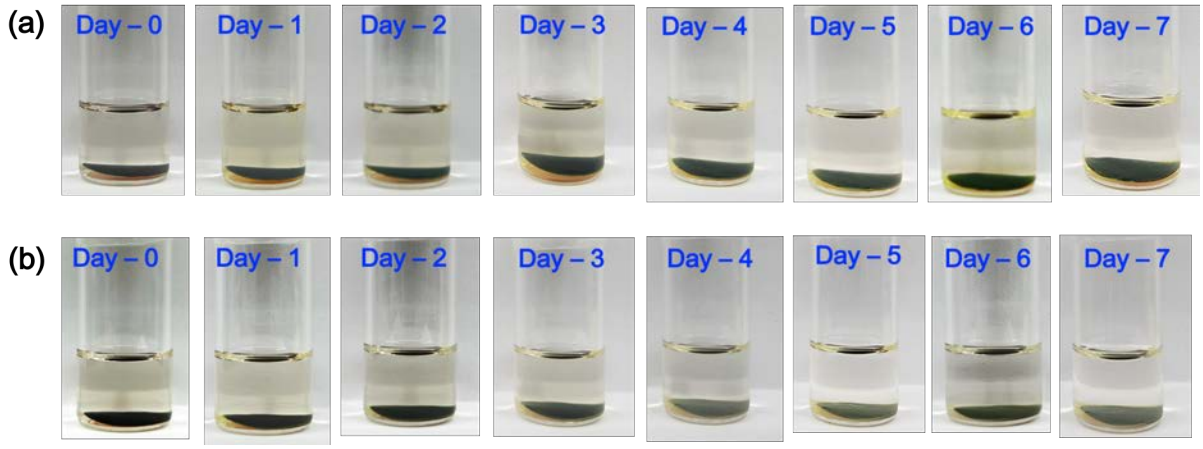

Fig. S19. Solubility test of **DiCN-Ether** with binder (a) and binder-free (b) in electrolyte.

Table S1. Inherent Viscosity and Solubility Behavior of Aramids

Polymer	η_{inh} (dL/g) [a]	Solubility in various Solvent[b]						
		NMP	DMAc	DMF	DMSO	*m*-Cresol	THF	$CHCl_3$
DiCN-Tpa	0.40	++	++	++	++	+	−	−
DiCN-Ether	0.68	++	++	++	++	+	−	−
DiCN-6F	2.07	++	++	++	++	+	+−	−

[a] Measured at a polymer concentration of 0.5 g/dL in DMAc at 30 °C.

[b] The solubility was determined with a 1 mg sample in 1 mL of a solvent. ++, soluble at room temperature; +, soluble on heating; +−, partially soluble or swelling; −, insoluble even on heating.

Table S2. Thermal Stability of Aramids

Polymer[a]	T_d^5 (°C)[b]		T_d^{10} (°C) [b]		R_{w800}[c] (%)
	N_2	Air	N_2	Air	
DiCN-Tpa	360	360	450	440	66
DiCN-Ether	355	350	430	420	62
DiCN-6F	375	370	490	490	61

[a] The polymer film samples were heated at 200 °C for 10 mins prior to all the thermal analyses.

[b] Temperature at which 5 % and 10% weight loss occurred, respectively, recorded by TGA at a heating rate of 20 °C/min and a gas flow rate of 20 cm^3/min.

[c] Residual weight percentages at 800 °C under nitrogen flow.

Table S3. EIS analysis results of aramid anodes (20 wt% of DiCN-aramids) at different cycling interval.

Active material	Stages	*R*s (Ω)	*R*ct (Ω)	D_{Li} (cm^2 s^{-1})
DiCN-Tpa	Before cycling	4.405	135.7	1.31×10^{-13}
	After 100 cycles	5.893	73.37	3.35×10^{-11}
DiCN-Ether	Before cycling	2.975	92.86	3.14×10^{-14}
	After 100 cycles	7.484	85.15	8.10×10^{-11}
DiCN-6F	Before cycling	4.064	145.1	1.44×10^{-14}
	After 100 cycles	4.009	158.1	1.32×10^{-12}

Table S4. EIS analysis results of DiCN-Ether and binder-free DiCN-Ether after 100 cycles.

Active material	*R*s (Ω)	*R*ct (Ω)	D_{Li} (cm^2 s^{-1})
DiCN-Ether (aramid:conductive carbon:PVDF = 40:50:10)	4.405	76.17	5.61×10^{-13}
Binder-free DiCN-Ether (aramid:conductive carbon = 50:50)	4.073	96.96	4.22×10^{-13}

Table S5. Summary of polymer-based LiB anodes.

Polymer type	Polymer name	Open Voltage (V vs. Li/Li^+)	Electrolytes	Current Density ($A\ g^{-1}$)	Specific Capacity ($mA\ h\ g^{-1}$)	Ref.
Conjugated pores polymer	Azo-BT (benzothiadiazole) Azo-Py (pyrene) Azo-Bz (Benzene)	0.005 – 3.0	1 M LiPF6 EC:DMC (1 : 1) (v/v)	0.5	725 (500 cycles) 619 (500 cycles) 503 (500 cycles)	14
	Polymer 4,7-dicarbazyl-[2,1,3]-benzothiadiazole (PDCzBT)	0.0 – 3.0	1 M LiPF6 EC:DMC:DEC (1 :1: 1) (v/v/v)	0.1 0.2	404 (100 cycles) 312 (400 cycles)	15
	Polydiaminophenylsulfone–Triazine	0.0 – 3.0	1 M LiPF6 EC:DEC (1 : 1) (v/v)	0.1 1	565 (100 cycles) 375 (100 cycles)	16
	SNW-1/CNTs	0.01 – 3.0	1 M LiPF6 EC:DMC:DEC (1 :1: 1) (v/v/v)	0.5	203 (1000 cycles)	17
Polyanhydride	Poly(dihydroanthracene succinic anhydride)	0.2 – 3.0	1 M LiPF6 EC:DMC (1 : 1) (v/v)	0.05	1100 (1000 cycles)	18
Polyazaacene	Poly(1,6-dihydropyrazino[2,3g]quinoxaline-2,3,8-triyl-7-(2H)-ylidene-7,8-dimethylidene)	0.0 – 3.0	1 M LiPF6 EC:DEC (1 : 1) (v/v)	0.1	1550 (100 cycles)	19
Polybenzimidazole	MPBI-550	0.1 – 3.0	1 M LiPF6 EC:DMC (1 : 1) (v/v) + 5 wt% FEC	1	700 (500 cycles)	20
Polystyrene	Hyper-crosslinked polystyrene (HPS)	0.0 – 3.0	1 M LiPF6 PC	0.2 2	356 (100 cycles) 222 (1000 cycles)	21
Polythiophene	P(C-TDPP-TA) P(F-TDPP-TA) P(C-TDPP-H) P(F-TDPP-H)	0.01 – 3.0	1 M LiPF6 EC:DMC (1 : 1) (v/v)	0.1	357 (500 cycles) 298 (500 cycles) 327 (500 cycles) 278 (500 cycles)	22
	DBD-CMP-1 DBD-CMP-2	0.005 – 3.0	1 M LiPF6 EC:DMC:EMC (1 :1: 1) (v/v/v)	0.1	315 (300 cycles) 595 (300 cycles)	23

Polymer type	Polymer name	Open Voltage (V vs. Li/Li^+)	Electrolytes	Current Density ($A\ g^{-1}$)	Specific Capacity ($mA\ h\ g^{-1}$)	Ref.
	poly(thiophene) (PT) poly(3,3'-bithiophene) (P33DT)	0.0 – 3.0	1 M LiPF6 EC:DMC:DEC (1 :1: 1) (v/v/v)	0.5	90 (1000 cycles) 663 (1000 cycles)	24
	PTp-COOH	0.01 – 3.0	1 M LiClO4 EC:DEC (1 : 1) (v/v)	0.5	147 (1000 cycles)	25
	Polytetra(2-thienyl)ethylene (PTTE)	0.005 – 3.0	1 M LiPF6 EC:DMC:EMC (1 :1: 1) (v/v/v)	0.5	585 (100 cycles)	26
	Poly-Triazine-Thiophene (PTT)-1 Poly-Triazine-Thiophene (PTT)-2 Poly-Triazine-Thiophene (PTT)-3 Poly-Triazine-Thiophene (PTT)-4	0.01 – 3.0	1 M LiPF6 EC:DMC (1 : 1) (v/v)	0.1	495 (300 cycles) 671 (300 cycles) 707 (300 cycles) 772 (300 cycles)	27
	P3-AQT	0.0 – 3.5	1 M LiPF6 EC:DMC:EMC (1 :1: 1) (v/v/v)	0.05 0.1 0.5 1	380 (100 cycles) 400 (100 cycles) 400 (100 cycles) 505 (100 cycles)	28
Polyimide	PMAQ	0.01 – 3.0	1 M LiPF6 EC:DMC:DEC (1 :1: 1) (v/v/v)	0.5	465 (150 cycles)	29
	PI	0.001 – 3.0	1 M LiPF6 EC:DMC (1 : 1) (v/v)	0.1	578 (50 cycles)	30
	PMTA	0.001 – 3.0	1 M LiPF6 EC:DMC (1 : 1) (v/v)	0.1	698 (50 cycles)	31
	Poly(imine-anthraquinone) (PIAQ)	0.01 – 3.5	1 M LiPF6 EC:DEC (1 : 1) (v/v)	0.2 1	1097 (100 cycles) 486 (1000 cycles)	32
	poly(benzobisimidazobenzophenanthroline) (BBL)	0.0 – 3.0	1 M LiPF6 EC:DEC (1 : 1) (v/v)	0.05	619 (100cycles)	33
	TPA-PMPI	0.02 – 3.0	1 M LiPF6 EC:DEC (1 : 1) (v/v)	0.1	1600 (100 cycles)	34
	N-CPIMs	0.0 – 3.0	1 M LiPF6 EC:DMC (1 : 1)	0.01	500 (5 cycles)	35

Polymer type	Polymer name	Open Voltage (V vs. Li/Li^+)	Electrolytes	Current Density ($A\ g^{-1}$)	Specific Capacity ($mA\ h\ g^{-1}$)	Ref.
			(v/v)			
Polyquinone	Polyanthraquinone-Triazine	0.01 – 3.0	1 M LiPF6 EC:DMC (1 : 1) (v/v)	0.2 1	1770 (400 cycles) 760 (400 cycles)	36
Aramids	**DiCN-Tpa**	0.02 – 3.0	1 M LiPF6 EC:DEC (1 : 1) (v/v)	0.1 2 5 10	1542 (100 cycles) 900 (1000 cycles) 651 (1000 cycles) 321 (1000 cycles)	**This Work**
	DiCN-Ether			0.1 2 5 10	1614 (100 cycles) 950 (1000 cycles) 686 (1000 cycles) 554 (1000 cycles)	
	DiCN-6F			0.1 2 5 10	1135 (100 cycles) 1100 (1000 cycles) 686 (1000 cycles) 414 (1000 cycles)	

Supplementary references:

1. T. Q. Nguyen and C. Breitkopf, *J. Electrochem. Soc.*, 2018, **165**, E826-E831.
2. T. Osaka, T. Momma, D. Mukoyama and H. Nara, *J. Power Sources*, 2012, **205**, 483-486.
3. H.-M. Cho, W.-S. Choi, J.-Y. Go, S.-E. Bae and H.-C. Shin, *J. Power Sources*, 2012, **198**, 273-280.
4. S. Rodrigues, N. Munichandraiah and A. K. Shukla, *J. Solid State Electrochem.*, 1999, **3**, 397-405.
5. E. Barsoukov and J. R. Macdonald, *Impedance Spectroscopy: Theory, Experiment, and Applications*, Wiley, 2018.
6. D. Aurbach, B. Markovsky, M. D. Levi, E. Levi, A. Schechter, M. Moshkovich and Y. Cohen, *J. Power Sources*, 1999, **81-82**, 95-111.
7. A. J. Bard and L. R. Faulkner, *Electrochemical Methods: Fundamentals and Applications, 2nd Edition*, Wiley Textbooks, 2000.
8. J. Wang, J. Polleux, J. Lim and B. Dunn, *J. Phys. Chem. C*, 2007, **111**, 14925-14931.
9. F.-F. Li, J.-F. Gao, Z.-H. He and L.-B. Kong, *ACS Appl. Energy Mater.*, 2020, **3**, 5448-5461.
10. V. Augustyn, J. Come, M. A. Lowe, J. W. Kim, P.-L. Taberna, S. H. Tolbert, H. D. Abruña, P. Simon and B. Dunn, *Nat. Mater.*, 2013, **12**, 518-522.
11. F. Yu, Z. Liu, R. Zhou, D. Tan, H. Wang and F. Wang, *Mater. Horiz.*, 2018, **5**, 529-535.
12. H. Lindström, S. Södergren, A. Solbrand, H. Rensmo, J. Hjelm, A. Hagfeldt and S.-E. Lindquist, *J. Phys. Chem. B*, 1997, **101**, 7717-7722.
13. T. C. Liu, *J. Electrochem. So.c*, 1998, **145**, 1882.
14. W. Ma, C. Zhang, X. Gao, C. Shu, C. Yan, F. Wang, Y. Chen, J. H. Zeng and J.-X. Jiang, *J. Power Sources*, 2020, **453**, 227868.
15. S. Zhang, W. Huang, P. Hu, C. Huang, C. Shang, C. Zhang, R. Yang and G. Cui, *J. Mater. Chem. A*, 2015, **3**, 1896-1901.
16. Q. Ma, J. Zheng, H. Kang, L. Zhang, Q. Zhang, H. Li, R. Wang, T. Zhou, Q. Chen, A. Liu, H. Li and C. Zhang, *ACS Appl. Mater. Interfaces*, 2021, **13**, 43002-43010.
17. S.-X. Xu, W. Xu, L.-J. Kong and Y.-H. Zhang, *SN Appl. Sci.*, 2020, **2**, 199.
18. D. Mukherjee, G. Gowda Y. K, H. Makri Nimbegondi Kotresh and S. Sampath, *ACS Appl. Mater. Interfaces*, 2017, **9**, 19446-19454.
19. J. Wu, X. Rui, G. Long, W. Chen, Q. Yan and Q. Zhang, *Angew. Chem. Int. Ed.*, 2015, **54**, 7354-7358.
20. S. Ren, L. Meng, C. Ma, Y. Yu, Y. Lou, D. Zhang, Y. Han, Z. Shi and S. Feng, *Chem. Eng. J.* 2021, **405**, 126621.
21. Z. Li, W. Zhong, A. Cheng, Z. Li, L. Li and H. Zhang, *Electrochim. Acta*, 2018, **281**, 162-169.
22. Z. Xu, S. Hou, Z. Zhu, P. Zhou, L. Xue, H. Lin, J. Zhou and S. Zhuo, *Nanoscale*, 2021, **13**, 2673-2684.
23. T. Yang, C. Zhang, W. Ma, X. Gao, C. Yan, F. Wang and J.-X. Jiang, *Solid State Ion.*, 2020, **347**, 115247.
24. C. Zhang, Y. He, P. Mu, X. Wang, Q. He, Y. Chen, J. Zeng, F. Wang, Y. Xu and J.-X. Jiang, *Adv. Funct. Mater.*, 2018, **28**, 1705432.
25. H. Numazawa, K. Sato, H. Imai and Y. Oaki, *NPG Asia Mater.*, 2018, **10**, 397-405.
26. X. Wang, C. Zhang, Y. Xu, Q. He, P. Mu, Y. Chen, J. Zeng, F. Wang and J.-X. Jiang, *Macromol. Chem. Phys.*, 2018, **219**, 1700524.
27. X. Xue, J. Luo, L. Kong, J. Zhao, Y. Zhang, H. Du, S. Chen and Y. Xie, *RSC Adv.*, 2021, **11**, 10688-10698.

28. C. Zhang, S. Chen, G. Zhou, Q. Hou, S. Luo, Y. Wang, G. Shi and R. Zeng, *J. Electroanal. Chem.* 2021, **895**, 115495.
29. Z. Ba, Z. Wang, Y. Zhou, H. Li, J. Dong, Q. Zhang and X. Zhao, *ACS Appl. Energy Mater.*, 2021, **4**, 13161-13171.
30. J. He, Y. Liao, Q. Hu, Z. Zeng, L. Yi, Y. Wang, H. Lu and M. Pan, *Ionics*, 2020, **26**, 3343-3350.
31. J. He, Y. Liao, Q. Hu, Z. Zeng, L. Yi, Y. Wang, H. Lu and M. Pan, *J. Power Sources*, 2020, **451**, 227792.
32. Z. Man, P. Li, D. Zhou, R. Zang, S. Wang, P. Li, S. Liu, X. Li, Y. Wu, X. Liang and G. Wang, *J. Mater. Chem. A*, 2019, **7**, 2368-2375.
33. J. Wu, X. Rui, C. Wang, W.-B. Pei, R. Lau, Q. Yan and Q. Zhang, *Adv. Energy Mater.*, 2015, **5**, 1402189.
34. K. B. Labasan, H.-J. Lin, F. Baskoro, J. J. H. Togonon, H. Q. Wong, C.-W. Chang, S. D. Arco and H.-J. Yen, *ACS Appl. Mater. Interfaces*, 2021, **13**, 17467-17477.
35. X. Han, P. Han, J. Yao, S. Zhang, X. Cao, J. Xiong, J. Zhang and G. Cui, *Electrochim. Acta*, 2016, **196**, 603-610.
36. H. Kang, H. Liu, C. Li, L. Sun, C. Zhang, H. Gao, J. Yin, B. Yang, Y. You, K.-C. Jiang, H. Long and S. Xin, *ACS Appl. Mater. Interfaces*, 2018, **10**, 37023-37030.